Invited Paper

# The Reuven Ramaty High Energy Solar Spectroscopic Imager (RHESSI) Mission

R. P. Lin[*a], B. Dennis[b], G. Hurford[a], D. M. Smith[a], A. Zehnder[c]
[a]Space Sciences Laboratory, Univ. of California/Berkeley, Berkeley, CA, USA 94720-7450
[b]NASA Goddard Space Flight Ctr., Greenbelt, MD, USA 20771
[c]Paul Scherrer Institut, Villigen PSI, Switzerland CH-5232

## ABSTRACT

The primary scientific objective of RHESSI Small Explorer mission is to investigate the physics of particle acceleration and energy release in solar flares, through imaging and spectroscopy of X-ray/gamma-ray continuum and gamma-ray lines emitted by accelerated electrons and ions, respectively. RHESSI utilizes rotating modulator collimators together with cooled germanium detectors to image X-rays/gamma-rays from 3 keV to 17 MeV. It provides the first hard X-ray imaging spectroscopy, the first high resolution spectroscopy of solar gamma-ray lines, and the first imaging of solar gamma-ray lines and continuum. Here we briefly describe the mission and instrumentation, and illustrate its capabilities with solar and cosmic observations obtained in the first 17 months of operation.

**Keywords:** solar flares, solar particle acceleration, solar X-ray/gamma-ray imaging, solar X-ray/gamma-ray spectroscopy

## 1. INTRODUCTION

The primary scientific objective of the Reuven Ramaty High Energy Solar Spectroscopic Imager (RHESSI) - the sixth NASA Small Explorer (SMEX) mission, is to investigate particle acceleration and explosive energy release in the magnetized plasmas at the Sun. The Sun is the most energetic particle accelerator in the solar system, accelerating ions up to tens of GeV and electrons to tens of MeV in solar flares and in fast Coronal Mass Ejections (CMEs). Solar flares are the most powerful explosions, releasing up to $10^{32}$-$10^{33}$ ergs in ~10-1000s. The flare-accelerated ~10-100 keV electrons (and sometimes >~1 MeV/nucleon ions) appear to contain a significant fraction, ~10-50%, of this energy, indicating that the particle acceleration and energy release processes are intimately linked. How the Sun releases this energy, presumably stored in the magnetic fields of the corona, and how it rapidly accelerates electrons and ions with such high efficiency, and to such high energies, is presently unknown.

High-energy emissions are the most direct signature of the acceleration of electrons, protons and heavier ions in solar flares. Bursts of bremsstrahlung hard X-rays emitted by accelerated electrons colliding with the ambient solar atmosphere, are the most common signature of the impulsive phase of a solar flare (Figure 1). Collisions of accelerated ions with the atmosphere result in a complex spectrum of narrow and broad gamma-ray lines. Hot (multi-million °K) thermal flare plasmas also emit bremsstrahlung X-rays.

RHESSI provides imaging and spectroscopy of hard X-ray/gamma-ray continua emitted by energetic electrons, and of gamma-ray lines produced by energetic ions including first high resolution hard X-ray imaging spectroscopy, the first high-resolution gamma-ray line spectroscopy, and the first imaging above 100 keV including the first imaging of gamma-ray lines. The spatial resolution is as fine as 2.3 arcsec with a full-Sun 1° field of view, and the spectral resolution is ~1-10 keV FWHM over the energy range from soft X-rays (3 keV) to gamma-rays (17 MeV).

RHESSI was launched on February 5, 2002, into a nearly circular, 38° inclination, 600-km altitude orbit and began continuous observations a week later. Over 8000 flares with detectable emission above 12 keV (>~600 above 25 keV) have been observed in the first year, including a gamma-ray line flare. Even more microflares have been detected above 3 keV. All the data is made immediately available to the scientific community, together with the analysis software (Schwartz et al., 2002).

* rlin@ssl..berkeley.edu; phone 1 510 642-1149; fax 1 510 643-8302; ssl.berkeley.edu



Telescopes and Instrumentation for Solar Astrophysics, edited by Silvano Fineschi, Mark A. Gummin,
Proceedings of SPIE Vol. 5171 (SPIE, Bellingham, WA, 2004) · 0277-786X/04/$15 · doi: 10.1117/12.506649

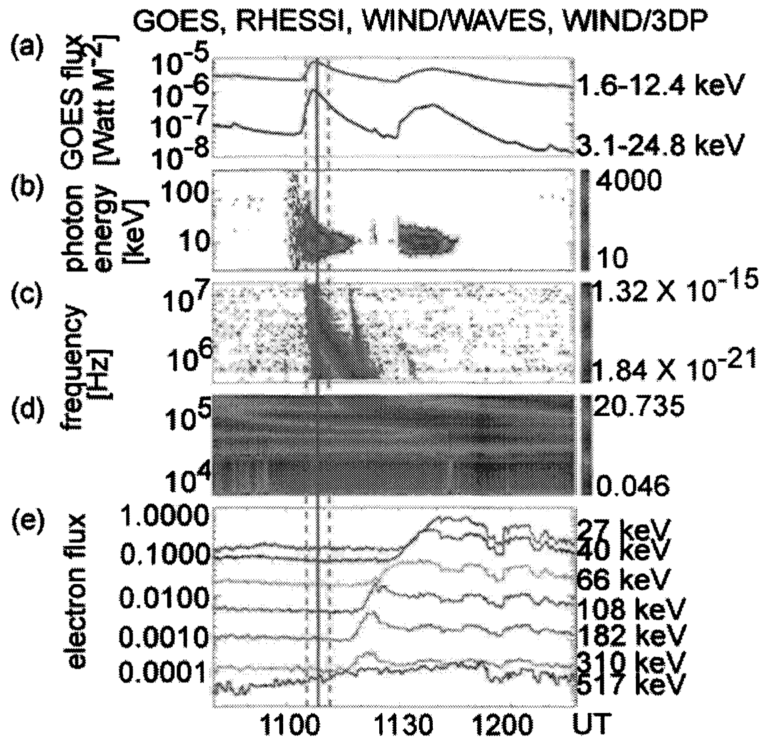


Figure 1. X-ray, and in-situ observations of energetic electrons: From top to bottom the panels show: GOES light curve, RHESSI x-ray spectrogram, WIND/WAVES radio spectrograms, and in-situ electron observations from WIND/3DP (Lin et al. 2002).

The RHESSI instrument utilizes a photon-based Fourier transform imaging technique, where every photon interaction is recorded with its energy and time of arrival. The high spectral resolution and the coverage down to 3 keV allow for the first time detailed measurement of the transition from thermal to non-thermal X-ray emission, essential for obtaining accurate energy measurements. RHESSI has 14 to 500 times more effective area than any previous solar instrument in the ~3 to 15 keV range, allowing it to detect microflares and quiet Sun emission with unprecedented sensitivity. It is also able to identify and image the Fe line complex at ~6.7 keV and the associated Fe-Ni feature at ~8 keV. Some of the new results (see the dedicated issue of Solar Physics (v. 210, November 2002) include:

* The first hard X-ray imaging spectroscopy of flares from thermal to non-thermal energies.
*The first flare high resolution X-ray spectroscopy that resolves the thermal-nonthermal energy transition, showing that the non-thermal power law extends down to <~10 keV and implying an energy content in the accelerated electrons at least several times greater than previous >~20 keV estimates.
* The discovery that flare non-thermal X-ray spectra often have a relatively sharp downward break, usually in the range ~30-50 keV for small flares but as high as >100 keV in large flares.
* The first high resolution flare gamma-ray line spectrum, measuring red-shifts of a fraction of a percent, implying directivity of the energetic ions as well as non-radial magnetic fields (Smith et al., 2003).
* The first imaging of flare gamma-ray lines, showing that the centroids of the energetic ion and electron sources are separated by ~20 arcsec (Hurford et al., 2003).
* The first detection of continuous glow from the Sun at 3-15 keV energies, with frequent microflaring. The microflare have non-thermal power-law spectra indicating substantial energy in accelerated electrons.
* The detection of a non-thermal coronal source with a double-power law spectrum during the onset of a large flare. This source requires a significant energy release into the corona prior to the impulsive phase (Lin et al., 2003).
* The detection of 3-15 keV X-ray emission from solar type III radio bursts, sometimes with no obvious relation to flares (Christe et al., 2003).
*The discovery of strong polarization in a cosmic gamma-ray burst, implying strong coherent magnetic fields in the source (Coburn and Boggs, 2003).

Here we briefly describe the RHESSI mission and instrument, and then illustrate its capabilities with solar and cosmic observations obtained in the first 17 months of operation.

## 2. INSTRUMENT AND MISSION DESCRIPTION

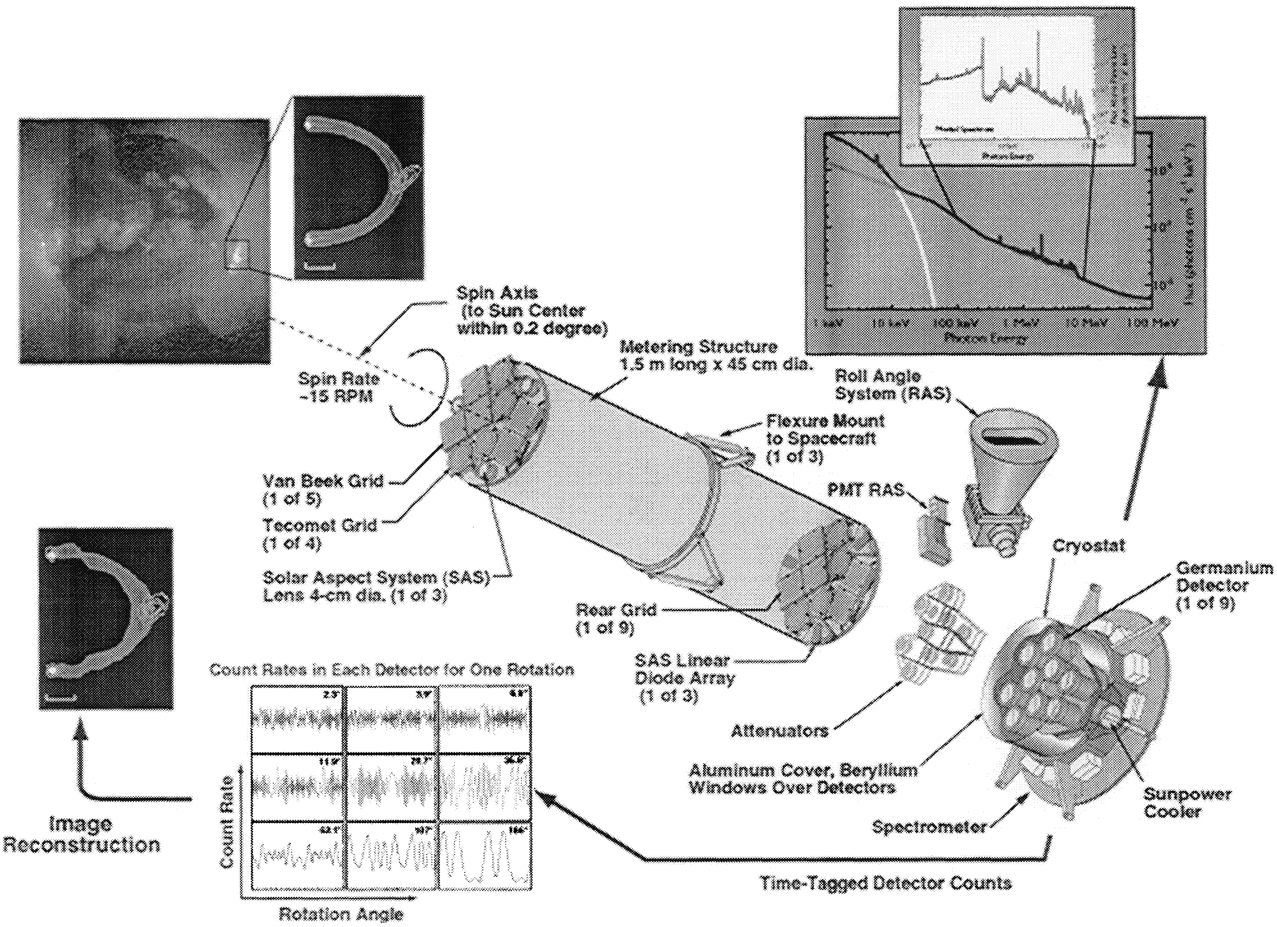


Figure 2. Schematic of the RHESSI instrument illustrating the imaging spectroscopy. X-rays and gamma-rays from the Sun (upper left) pass through the slits of the front and rear grids of each of the nine grid pairs to reach the germanium detector (Lin et al., 2002). As the spacecraft rotates the detector count rates are temporally modulated (lower left). These modulations can be analyzed to reconstruct the image. The germanium detectors are cryogenically cooled to provide high spectral resolution capable of resolving narrow gamma-ray lines and steep solar continuum spectra (upper right). The attenuators are inserted automatically when the count rate approaches saturation. The SAS,RAS and PMTRAS provide solar pointing and roll aspect information.

A detailed description of the RHESSI imaging technique is given in Hurford et al. (2002). At hard X-ray and gamma-ray energies, unlike soft X-rays, EUV, and longer wavelength emissions, focusing optics are not feasible. The only viable method of obtaining arcsecond-class images in hard X-rays and gamma-rays within the SMEX constraints is with Fourier-transform imaging, similar to that used in the pioneering Hinotori rotating modulation collimator (Makishima et al., 1977) and Yohkoh Hard X-ray Telescope (HXT) (Kosugi et al., 1991). The RHESSI instrument (Figure 2) has an imager made up of nine Rotating Modulation Collimators (RMCs), each consisting of a pair of widely separated grids mounted on a rotating spacecraft, to achieve angular resolution of ~2 arcsec for hard X-rays and imaging with ~35 arsec up to gamma-ray energies. Behind each RMC is a segmented germanium detector (GeD) to detect photons from 3 keV to 17 MeV. The GeDs are cooled to ~75 K by a space-qualified long-life mechanical cryocooler, to achieve the highest spectral resolution of any presently available gamma-ray detector. An automated shutter system allows a wide dynamic range ($>10^7$) of flare intensities to be handled without instrument saturation.

As the spacecraft rotates, the RMCs convert the spatial information from the source into temporal modulation of the photon counting rates of the GeDs. For a parallel incident beam, the modulated waveform generated by a smoothly rotating spacecraft has a distinctive quasi-triangular shape locally. The amplitude is proportional to the intensity of the beam, and the phase and frequency depend on the direction of incidence. For complex sources, and over small rotation angles, the amplitude and phase of the waveform provide a direct measurement of a single Fourier component of the angular distribution of the source (e.g., Prince et al., 1988). Different Fourier components are measured at different rotation angles and with grids of different pitches. For RHESSI, the separation between grids in each RMC is L = 1.55 m and the grid pitches range from p=34 $\mu$m to 2.75 mm in steps of $\sqrt{3}$. This provides angular resolutions spaced logarithmically from 2.3 arcsec to >~3 arcmin, allowing sources to be imaged over a wide range of angular scales. Diffuse sources larger than 3 arcmin are not imaged but full spectroscopic information is still obtained. Multiple smaller sources are imaged regardless of their separation.

In a half rotation (2 s), the nine RMCs measure amplitudes and phases of ~1100 Fourier components for a typical source location. Although one half rotation is required to measure a full set of Fourier components, the measurement of each component takes only a single modulation cycle, which can be as short as 1.3 ms for the finest grids. Thus, when count rates are sufficiently high, crude images (from about ten Fourier components) can be obtained, in principle, on timescales of tens of milliseconds. A Solar Aspect System (SAS) (Zehnder et al., 2002) provides pitch and yaw measurements relative to the solar limbs to arcsecond accuracy on time scales of tens of ms. Two redundant Roll Angle Systems -- a CCD-based version (CCD RAS) and a photomultiplier-based version (PMT RAS) -- that each provide the roll angle to arcminute accuracy several times per rotation with respect to the fixed stars (Hurford and Curtis, 2002).

Changing the separation (L) between grids or displacing the grids parallel to the slits has little effect on imaging performance. A relative displacement perpendicular to the slits affects the phase but not the amplitude of modulation. Any such displacement will be accurately monitored by the SAS, and can be fully compensated for in the image reconstruction process. The critical alignment requirement is associated with the rotation or twist of one grid with respect to the other about the line of sight to the source. A relative twist of p/D (D = diameter of grid) reduces the modulated amplitude almost to zero. To minimize twist, the grids are aligned and mounted precisely on grid trays which are attached to opposite ends of a graphite-epoxy support tube. For the finest grids (2.3 arcsec resolution) a 1-arcmin alignment is needed. Thus, HESSI can achieve arcsec-quality images with an instrument having only arcmin alignment requirements. The energy and time (to a microsecond) of every photon interaction, together with SAS and RAS data, are recorded in the spacecraft's on-board 4-Gbyte solid-state memory (sized to hold all the data from the largest flare) and automatically telemetered to the ground within 48 hours. With these data, the X-ray/gamma-ray images can be reconstructed on the ground.

The instrument's ~1° field of view is much wider than the ~0.5° solar diameter, so all flares are detected, and pointing can be automated. The spin-stabilized (~15 rpm) spacecraft is Sun-pointing to within ~0.2° and operates autonomously. The mission is operated from Berkeley using a dedicated 11-m antenna for telemetry reception and command uplinks.

## 3. SCIENCE

### 3.1 Electron Acceleration and Energy Release in Solar Flares

Figure 3a shows one of the first examples of RHESSI imaging spectroscopy, for the 20 Feb '0 flare. Images are shown in 2 keV bands from 12 to 26 keV, and then broader bands up to 80 keV. The image evolves from an elongated single source at low energies to two footpoints at high energies. Figure 3b shows high-resolution (~1 keV FWHM) X-ray spectra for the flare, showing the thermal (~10 MK) component dominating at low energies, with a power-law component dominating at high energies.

If the electrons producing the power-law X-rays have energies, $E_e$, much greater than the average thermal energy, kT, of the ambient gas, then essentially all of the electron energy will be lost to Coulomb collisions, with only a tiny fraction ~10^-5 lost to bremsstrahlung. For this non-thermal situation, it was found that in many flares to produce the observed hard X-ray fluxes, the energy in accelerated >20 keV electrons must be comparable to the total flare radiative and mechanical output (Lin and Hudson 1976). Thus, the acceleration of electrons to tens of keV may be the most direct consequence of the basic flare-energy release process.

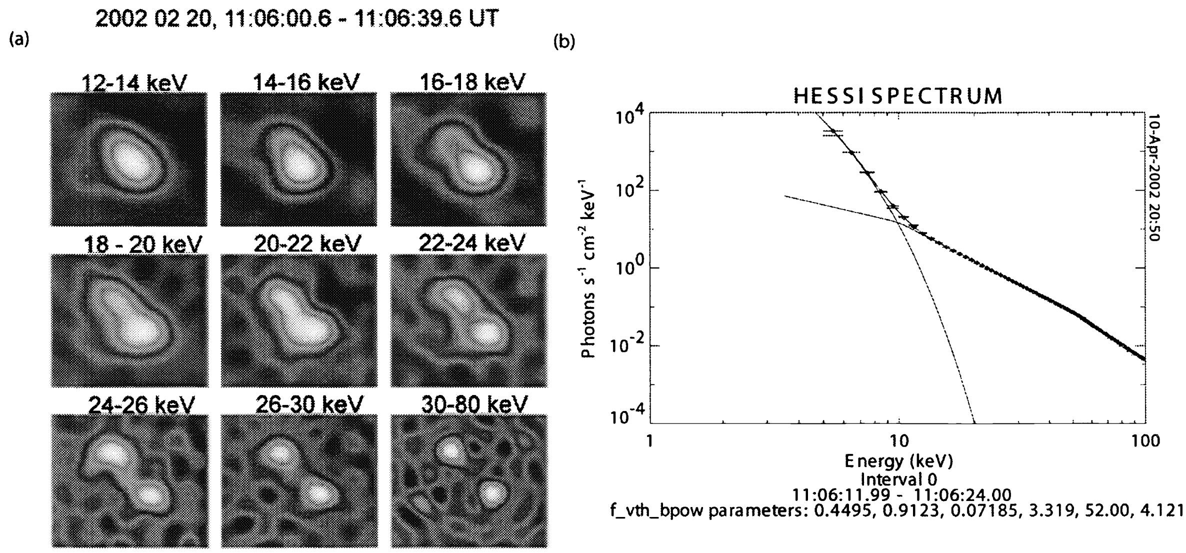


Figure 3. (a) RHESSI Imaging spectroscopy of the February 20, 2002 flare. Images (64" X 64") at different energies are shown (Lin et al., 2002). The spatial resolution is 8". (b) RHESSI X-ray spectrum of the same flare. A thermal and a broken power law are fitted to the observed spatially integrated spectrum.

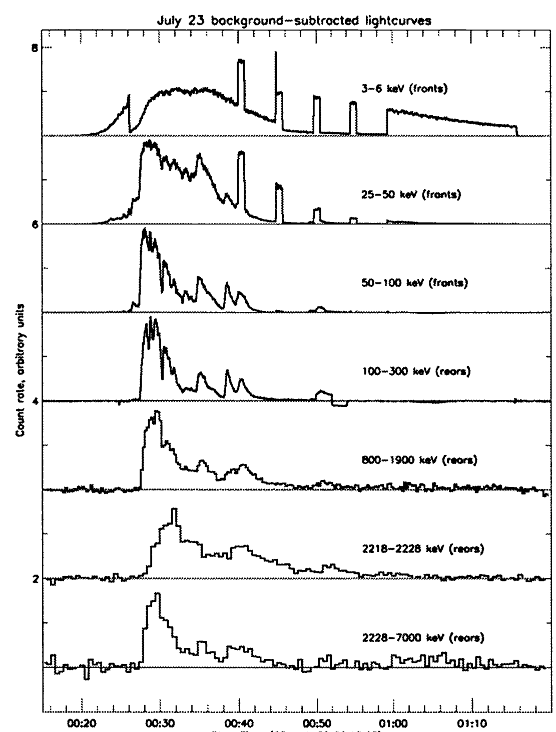


Figure 4. Background-subtracted light curves for the July 23, 2002 gamma-ray flare at 7 different energies.

Earlier solar hard X-ray instruments flown in space had relatively poor energy resolution most were designed with a thick entrance window to eliminate photons below ~20 or 25 keV to avoid pile-up and saturation from low energy thermal photons (Kane and Anderson, 1970). Thus, previous estimates of the total energy in electrons referred to electrons above 20 or 25 keV. RHESSI is the first space experiment capable of accurately measuring the flare spectrum from thermal to non-thermal. As Figure 3b shows, the non-thermal power-law spectrum extends down to ~10 keV, implying that the energy contained in the electrons is at least several times greater than estimated previously. In fact, since we are now interested in the energy loss of electrons for which $E_e$ is only several times kT, the Coulomb losses need to be evaluated more carefully. This case of a warm plasma has been addressed by Emslie (2003).

The precise RHESSI observations (Figure 3b) clearly show that the non-thermal spectrum is double-power-law, with a relatively sharp downward break at ~40 keV; a similar break was first seen in the high resolution flare spectrum obtained by a balloon-borne germanium instrument (Lin et al. 1981). What is the cause of this break? Several possible interpretations have been suggested: a break in the parent electron spectrum due to the acceleration process; it could result from non-uniform target ionization: the higher energy electrons penetrating to the neutral chromosphere while the lower energy electrons stop in the fully ionized corona where their Coulomb energy loss rate is ~3 times higher (Brown et al., 2002); or it might be due to beam-plasma return current effects (Gordovsky and Zharkova, 2003); or some as yet unknown process. More detailed analysis will be required to get to the origin of this break.

### 3.1.1 The X4.8 flare of July 23, 2002

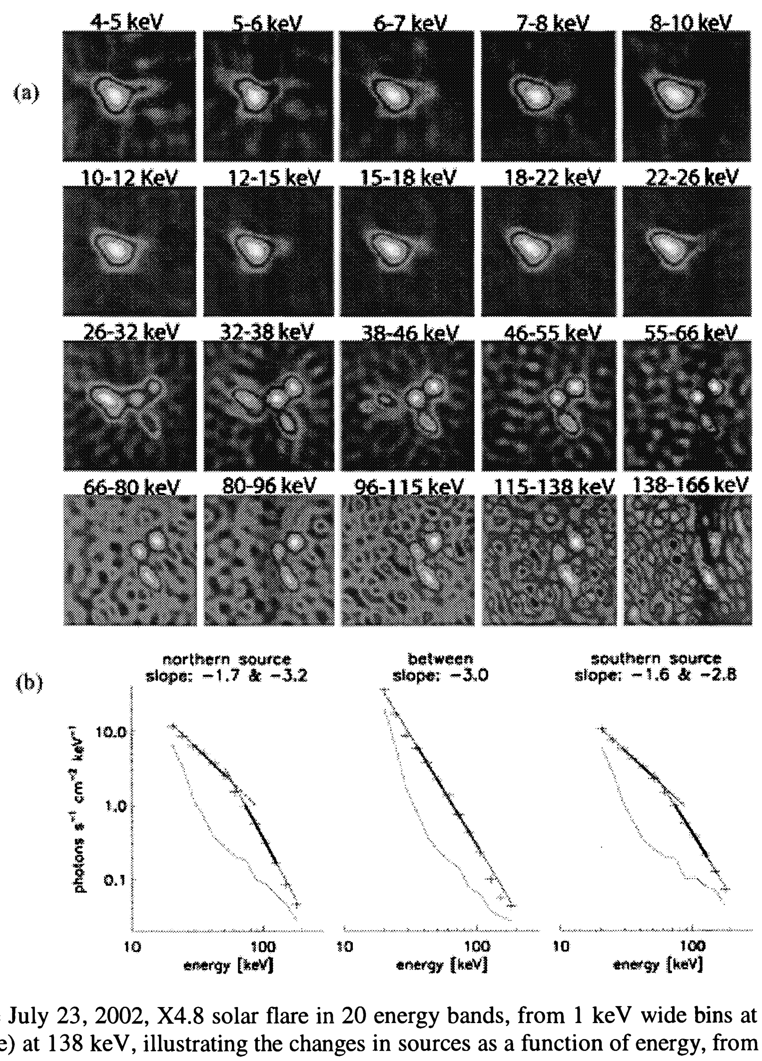


Figure 5. a) Imaging of the July 23, 2002, X4.8 solar flare in 20 energy bands, from 1 keV wide bins at 4 keV, to 28 keV wide bins (for enough counts to image) at 138 keV, illustrating the changes in sources as a function of energy, from a single dominant elongated source at energies below ~30 keV to three sources above ~40 keV (Krucker et al., 2003). The images are 64 arcseconds on a side; the lower left corner is just at the southeast limb of the Sun. b) The energy spectra of the three dominant sources at energies above ~40

keV, showing that the spectra are similar for the north and south sources but quite different for the source in between (Emslies et al., 2003). The dashed lines indicate background.

The most powerful flare and the first gamma-ray line flare observed by RHESSI the X4.8 flare of 23 July 2002 located at S13E72 has yielded a harvest of new results (see Astrophysical Journal Letters, v, 2003). The flare hard X-ray and gamma-ray emission (Figure 4) divide naturally into an rise phase (~0018 to ~0027UT) dominated by a coronal hard X-ray source that appears to be non-thermal, a main impulsive phase (~0027 to ~0043 UT) with continuum and gamma-ray line emission extending up to >~7 MeV, and a decay phase (>~0043UT) dominated by a superhot (~40 million degrees) thermal hard X-ray source.

During the rise the hard X-ray emission above 10 keV is concentrated in a coronal source with no counterpart observed in TRACE 195 A, SoHO MDI visible or Halpha images (Lin et al 2003). The hard x-ray spectrum above ~10 keV fits to a double-power-law spectral shape (Holman et al 2003).

Assuming thick target emission from energetic electrons colliding with a cold ambient medium ($E_e$>>kT), the energy deposited by the electrons above ~10 keV, integrating over time from the rise to ~0026UT, is >~4x$10^{32}$ ergs. But by fitting the observed spectrum to a thermal component plus a power-law non-thermal component and choosing the highest possible low energy cutoff (~20 keV) to the non-thermal electron spectrum that is consistent with the X-ray data, Holman et al finds a lower limit to the total energy input in accelerated electrons of ~2x$10^{31}$ ergs. Thus, very substantial energy release and acceleration of electrons occurs high in the corona prior to the impulsive phase.

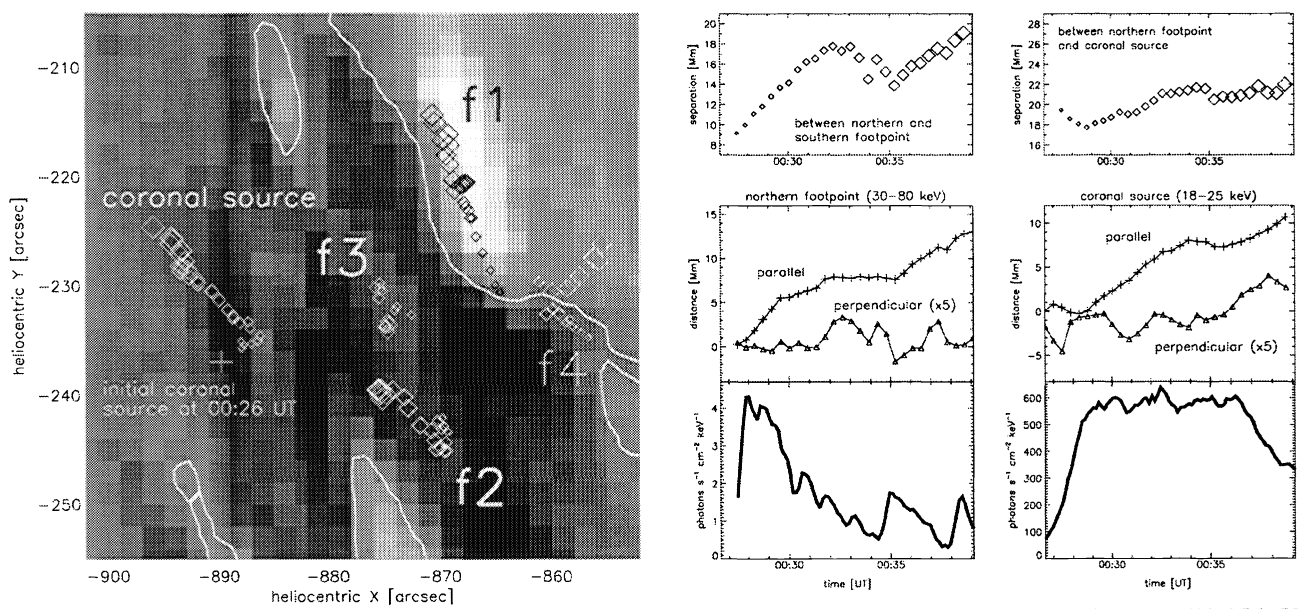

Figure 6. Left: Temporal evolution of centroids of HXR sources f1, f2, f3, and f4 (30-80 keV) and the coronal sources (18-25 keV) taken from 27 s integrated images (Krucker et al, 2003). The size of the diamonds represent time (00:26:55UT - 00:39:07UT). The gray-scale image is a SOHO MDI magnetogram. The apparent neutral line is shown in white. Right: Relative separation versus time of the two main footpoints f1 and f2. Below: Source motion of f1 (right) and the coronal source (left). The source motion parallel (crosses) and perpendicular (triangles, multiplied by 5) to the main direction of motion and the total flux are shown.

At the beginning of the impulsive phase, ~0027UT, there is an abrupt change in the character of the hard X-ray emission, to strong footpoint emission (Krucker et al., 2003) together with a (super)hot thermal source in the corona. Three footpoints are observed - a north, a south, and a middle footpoint - each with a chromospheric counterpart observed in Hα and TRACE (Figure 5). Their spectra, although still double-power-law, are much harder than the rise phase coronal source. During the first (and most intense) burst, the north footpoint rapidly moves northeast, roughly parallel to the magnetic neutral line, while the south footpoint stays relatively stationary, so the separation between them increases with time (Figure 6). These X-ray fluxes and spectra of the north and south footpoints show the same temporal variations, suggesting that they are at opposite ends of the same magnetic loop. The motions generally are most rapid when the X-ray flux is largest, as might be expected if magnetic reconnection is forming the loops connecting the footpoints.

Of particular interest for flare energy release are the recent simulations of collisionless reconnection in 3D that indicate electron acceleration is a major consequence of the process (Drake et al., 2003), and the observation by the Wind spacecraft of electrons accelerated to hundreds of keV energy in the magnetic reconnection ion diffusion region in the distant magnetotail (Oieroset et al., 2002).

### 3.2 Ion Acceleration and Gamma-ray Line Emission

RHESSI has provided the first direct information on the location and spatial characteristics of the accelerated ions in a flare, by imaging the gamma-ray line emission produced by collisions of the energetic (tens of MeV) ions with the ambient solar atmosphere (Hurford et al., 2003). The two rotating modulation collimators (35 & 180 arcsec resolution) with the thickest (2 & 3 cm, respectively) tungsten grids were used to obtain images of the narrow deuterium line at 2.223 MeV formed by thermalization and capture of neutrons produced in the collisions, the 3.25-6.5 MeV band that includes the prompt de-excitation lines of C and O, and the 0.3-0.5 and 0.7-1.4 MeV bands that are dominated by electron-bremsstrahlung, all for the same time interval.

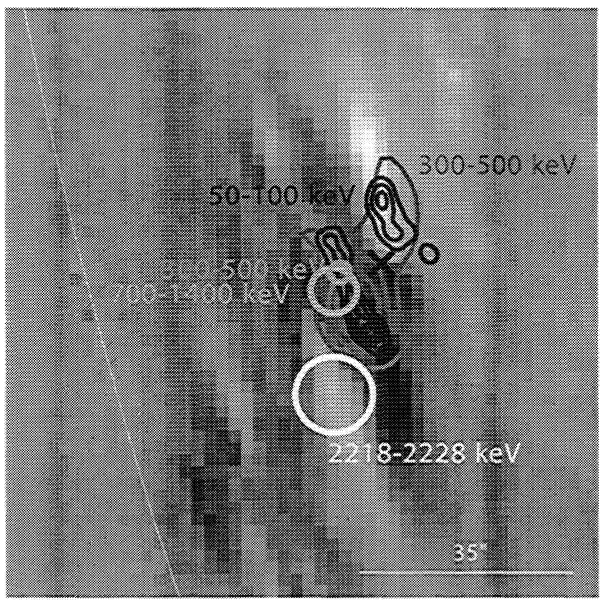


Figure 7. Location of the gamma-ray source for the 23 July 2003 flare (Hurford et al, 2003). The circles represent the 1-sigma errors for the energies given. All these images are made with identical imaging parameters. The FWHM angular resolution is shown in the lower right. Blue contours show the high resolution 50-100 keV map at 3" resolution and the red contours represents the 300-500 keV map with 8" resolution. The blue X shows the centroid of the 50-100 keV emission made with the same lower resolution as the gamma-ray maps. The background image is a SOHO/MDI magnetogram.

The centroid of the 2.223 MeV image (Figure 7) was found to be displaced by ~20(+-6) arcsec (~15,000 km) from that of the 300-500 keV band (and from the 50-100 keV x-ray continuum emission), implying a difference in acceleration and/or propagation between the accelerated electron and ion populations near the Sun. If the acceleration process is indeed common, as suggested by the similarity (within ~5 s) of the time profiles of the prompt gamma-ray line emission and the bremsstrahlung X-ray/gamma-ray continuum emission, it would suggest that electric fields may be involved.

The de-excitation lines, which come from ambient nuclei stimulated by accelerated protons and alpha particles, were measured for the first time with high spectral resolution (Figure 8) (Smith et al., 2003). They were discovered to be significantly redshifted, by fractions of a percent, even though the flare was nearly on the solar limb. These redshifts imply that the magnetic loop containing the ions must have been strongly tilted from radial, toward the solar surface.
Also resolved for the first time in this flare was the positron-annihilation line which was discovered to be unexpectedly broad (8.1 keV; Share et al., 2003). This width implies annihilation in either a hot medium of about 600,000K or a cold

medium very close to 6000K. The quiet solar atmosphere contains little material at either temperature; thus this line is a very sensitive measure of some very unusual conditions associated with flares.

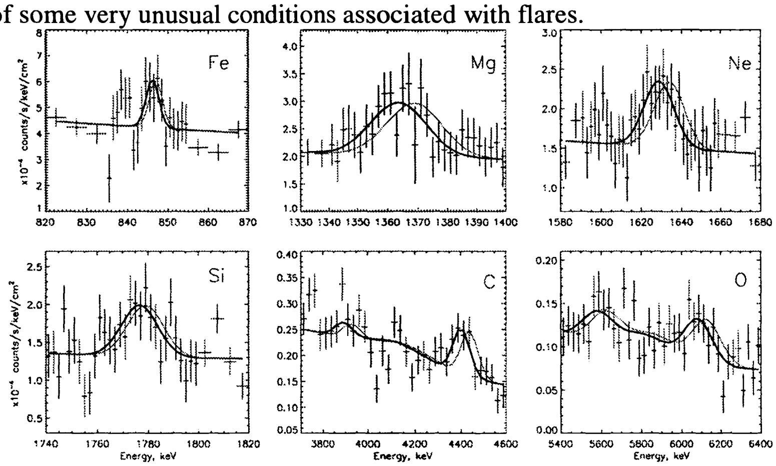


Figure 8. RHESSI background-subtracted count spectra from 00:27:20UT to 00:43:20UT on 23 July, 2002 (Smith et al., 2003). Each panel is labeled with the element primarily responsible for the line shown. The carbon and oxygen lines also show the secondary peak from escape of a 511 keV positron-annihilation photon, which also contains information on the line shape. The heavy cube shown in each panel a Gaussian fit plus the underlying bremsstrahlung continuum and broad lines, convolved with the instrument response. The lighter line is the same fit forced to zero redshift for comparison. The error bars are from Poisson statistics.

### 3.3 Flare/CME Associations

Given the geoeffectiveness of CMEs, the effort to understand and eventually to predict these powerful solar events has become a major objective for solar physics. Observations with TRACE, Yohkoh/SXT, and SOHO/EIT and UVCS have revealed the early stages of CMEs, while LASCO images show the CMEs propagating out into interplanetary space. Instruments on ACE, Wind, and SOHO detect the CME and its shock at ~ 1AU.

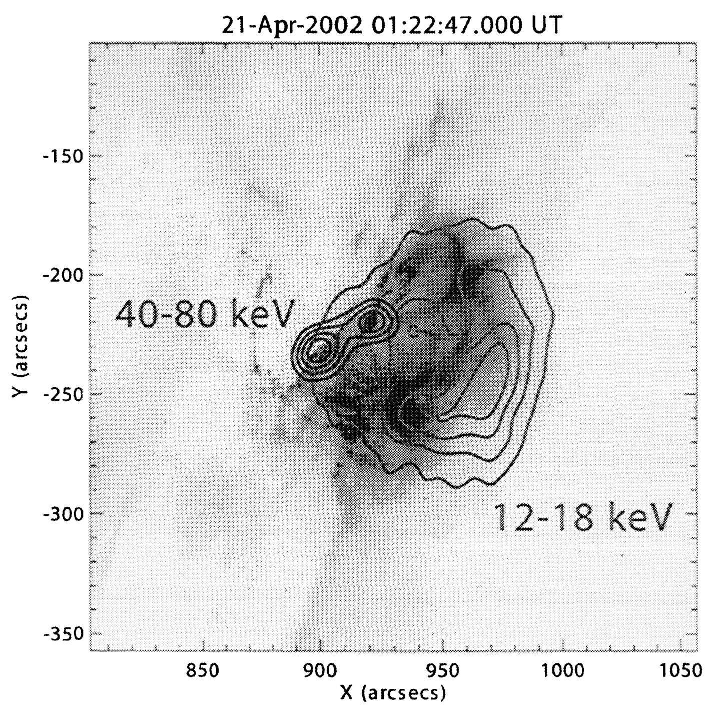

Figure 9. RHESSI and TRACE EUV observations of the X1.5 class flare on April 21, 2002 (Gallagher et al., 2002). Contours at 12-18 keV and 40-80 keV are shown. Contour levels are 30, 50, 70, 90%.

Despite these observations, little is understood about the early initiation of a CME and its connection to the very large energy release of the often-associated flares. RHESSI has provided observations of several such associated flares in which 1032 ergs or more appear in the nonthermal electrons alone on time scales of minutes during the period of CME initiation and acceleration. The flare/CME event on 21 April 2002 is the best-observed example of such an association.

The first hard X-ray emission on 21 April 2002 was detected with RHESSI some 5 minutes before any brightening was observed in the TRACE 19.5-nm images (Gallagher et al., 2002). This time delay is presumably because the early hot plasma was at a higher temperature than the ~1.5 MK sensitive range of the TRACE passband. The hard X-ray emission continued to rise for the following hour, at the same time that a wave-like propagation appeared to move through the TRACE field at a mean velocity of ~120 km/s. This has been interpreted by Gallagher et al. (2003) as the first evidence for the CME.

Thanks in part to the early warning made by the RHESSI-funded Max Millennium flare forecasters, UVCS recorded the passage of the CME through its slit that was fortuitously placed 1.63 solar radii off the limb. LASCO obtained four images of the CME as it passed through its C2 and C3 fields. Gallagher et al. (2003) combined these CME observations to show that from the CME initiation in near coincidence with the start of the associated flare, the leading edge accelerated to a maximum velocity of over 2500 km/s in less than 2 hours. The maximum rate of acceleration was as high as 1500 m/s2 and this occurred when hard X-ray emission was seen with RHESSI. The flare released some $10^{32}$ ergs during its rise phase over the same time period that the CME was being accelerated. An intense SEP event was seen at the Earth.

With its high sensitivity to X-rays below 10 keV, RHESSI was able to follow the decay phase of this event for over 12 hours. The RHESSI images (Figure 9) show a bright X-ray source, some 30" in extent, moving out above the limb with a velocity that was initially about 10 km/s, but decreased to about 2 km/s after 2 hours, and then maintained that value for another 10 hours. Images made at different energies showed that the higher energy emissions (6–12 keV) consistently came from slightly higher altitude than the lower energies (3–6 keV). This result provides support for the basic Kopp and Pneuman flare model in which energy is released at higher and higher altitudes in the corona as the flare progresses, energizing larger and larger magnetic loops (Gallagher et al., 2002).

The 23 July 2002 (Lin et al. 2003) flare was considerably more energetic than that on 21 April and produced emission detectable with RHESSI into the MeV range, including many nuclear gamma-ray lines, as discussed earlier. A fast (2180 km/s) CME was also recorded in association with this flare but no SEP event was seen at the Earth above the elevated background from the July 20 CME, that was itself accompanied by a flare but not observed with RHESSI.

### 3.4 Microflares and the Quiet Sun

The Sun releases energy in transient outbursts, ranging from major flares down to microflares and even nanoflares, with the frequency of the releases increasing as the energy released decreases (see discussion in Aschwanden et al., 2000). For flares, the energy releases often appear to be dominated by accelerated 10s of keV electrons and sometimes MeV/nucleon ions. Hard X-ray microflares, tiny bursts with 1027 to 1028 ergs in >20-keV electrons, were discovered to occur on average once every ~6~minutes near solar maximum (Lin et al., 1984), leading to speculation that the energy released in accelerated electrons, summed over HXR bursts of all sizes, might contribute significantly to the heating of the active corona.

Using the BATSE SPEC detectors on the Compton Gamma-Ray Observatory, whose thresholds were occasionally set as low as 8~keV, Lin et al. (2001) found that only one third of all non-thermal (hard spectra unlikely to be thermal) events detected above 8 keV are observed above 25~keV. Additionally, the generally steep HXR spectra (power-law fits with exponent of 3-7) reveal that most of the flare energy is in the non-thermal electrons at lowest energy. Furthermore, the similarity of frequency vs. energy release distribution of these >8keV bursts to that of active region transient brightenings (ARTBs) seen in soft X-rays by the Yohkoh SXT instrument (Shimizu, 1995) suggests that these accelerated electrons may provide the energy for ARTBs.

The excellent sensitivity, spectral and spatial resolution provided by RHESSI allows for the first time the detailed study of the locations and the spectra of solar microflares down to 3 keV. Previous solar hard X-ray instruments have entrance windows that absorb emission below ~15-25 keV to avoid pile-up and saturation from the intense thermal emissions in large flares (Kane and Anderson, 1970). The RHESSI instrument accommodates medium and large flares by automatically inserting shutters in front of detectors to absorb low energy photons and avoid saturation. Compared to the most sensitive previous instrument from 3 to 15 keV, the Hard X-ray Imaging Spectrometer (HXIS) on SMM, RHESSI with the shutters out (Figure 3c) has an effective area 14 to 500 times larger. Thus, RHESSI can probe the Sun in the 3-15 keV energy range with unprecedented sensitivity to provide new information on low level energy releases and quiet Sun emissions, whether they result in heating of >~5 x $10^6$ K thermal plasmas or in the acceleration of low energy electrons.

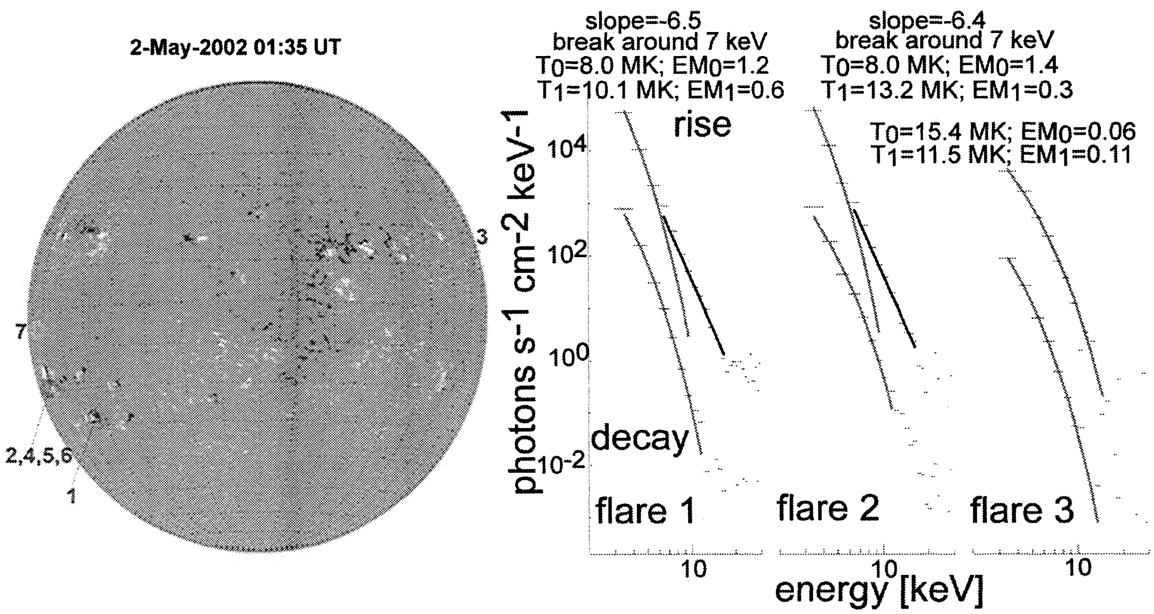


Figure 10. (left) Locations of the 7 largest microflares (GOES class A6 and smaller) observed during May 2, 2002, 1:40-2:40 UT (Krucker and Lin, 2002). (right) Spectra during the impulsive phase (shown shifted up by two decades) and the decay phase of the microflares labeled 1 to 3 in the figure to the right. The impulsive phase is fitted with both a thermal (light gray) and a non-thermal (dark gray) component, the decay phase with a thermal component only. For the behind-the-limb microflare (flare 3), a thermal alone fits the data well enough. The shown colored curves give the range fitted; values above ~15 keV are dominated by noise.

The first RHESSI results on active region microflares (Figure 10) show soft (power law exponents between 4 and 7) non-thermal spectra down to low (<~7 keV) energies (Benz & Grigis, 2002; Krucker et al., 2002). If a 25 keV cutoff energy is assumed, the total energy in non-thermal electrons in microflares is underestimated by at least a factor of ~10, in some events up to a factor of ~2000. Furthermore, the smaller the event, the steeper the spectrum appears to be. Thus there may be a systematic underestimate of the energy in small events relative to large events, and the frequency distribution of microflares may well be steeper than previously reported (Crosby et al., 1993), i.e. microflare heating might contribute more to coronal heating than previously thought. A detailed statistical study is underway.

As the total solar emission in this energy range declines, it will be possible to see even smaller events than during the first years of the mission, possibly down to the micro/nanoflares where perhaps most of the non-thermal energy is released.

Towards solar minimum, it will be also possible to study the emission of the 'quiet' Sun (when no obvious microflares are seen) by time averaging RHESSI observations over many hours. Such imaging spectroscopy of the quiet Sun in the 3-15 keV range may reveal insights on the possible non-thermal nature of the quiet Sun emission that could be related to unresolved micro/nanoflares of even smaller size.

### 3.5 Solar Energetic Particles (SEPs)

SEP events observed in the IPM have been classified as impulsive or gradual, so-called because of the temporal behavior of the associated flare soft X-ray burst (Lin 1987, 1994). Impulsive events (Lin, 1985) are dominated by non-relativistic electrons, ~1 to 10s of keV (but sometimes down to ~0.1 keV, or up to 100s of keV). They are the most commonly observed solar events at 1 AU (>~1000/year near solar maximum over entire Sun). Impulsive electron events are observed to be emitted over a cone of ~40-60° of solar longitude, and they are often closely associated with type III radio bursts, and sometimes with small flares, usually too small to detect gamma-ray lines. The associated energetic ion emission is generally weak and limited to low energies (<~1 MeV/nucleon), but typically $^3$He-rich (Reames et al. 1985) and heavy ion-rich (Fe, Mg, Si, S). Surprisingly, gamma-ray de-excitation line measurements show that the energetic ions in *large* flares are often also $^3$He-rich (Mandzhavidze et al., 1999) and Fe-rich (Murphy et al., 1991).

Gradual SEP events (tens per year at solar max) are generally large (hence also called LSEP) events dominated by protons, with "normal" solar abundance and charge states typical of quiet 1-2 x $10^6$ K corona, (e.g. $Fe^{+13}$). They extend over >100° in longitude and are usually associated with large flares (sometimes absent) and fast, wide Coronal Mass Ejections (CME's). The SEPs in gradual events are generally believed to be accelerated at altitudes of a few to ~tens of solar radii by the fast shocks driven by the CMEs (Kahler, 1999, Reames 1996), but acceleration processes in the high corona (Klein and Trottet, 2001, Cane 2002), or acceleration due to interactions between CMEs (Golpaswamy 2002), or flare acceleration processes have also been proposed. Recent ACE observations, for example, show significant enrichments of 3He and Fe in some *gradual* events, more than can be easily explained as acceleration of remnant 3He and Fe in the IPM from previous impulsive events.

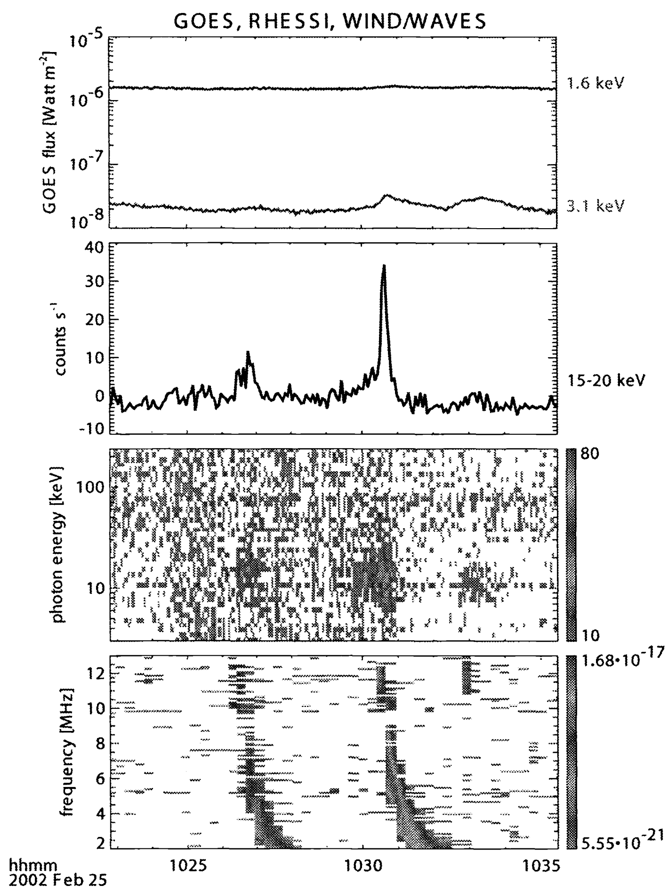


Figure 11. X-ray and radio observations of two small events. From top to bottom, GOES lightcurves, RHESSI 15-20 keV lightcurve, RHESSI x-ray spectrogram, and WIND/WAVES radio spectrogram are shown. The electron acceleration happens most likely in the corona; downward moving energetic electrons produce HXR emission in the lower, denser corona, while escaping electron beams emit radio type III bursts.

Most of the flare hard X-ray emissions observed by RHESSI come from energetic electrons colliding with the dense lower solar atmosphere. In an initial survey of more than 600 HXR events detected by RHESSI (Rauscher et al. 2002) about 70% were accompanied by interplanetary type III bursts seen by WIND/WAVES. The impulsive event electrons that escape through the relatively low density corona and IPM to produce the type III radio bursts will also produce bremsstrahlung hard X-rays, albeit at much lower fluxes.

The energy spectra of the impulsive event/type III electrons observed in the IPM are power-laws, often extending down to ~1 keV before a turnover, indicating a high coronal origin (Lin et al. 1996). With RHESSI's high sensitivity down to 3 keV, very weak HXR events are sometimes observed which are simultaneous with the type III burst but either do not have the usual intense flare HXR emission or the flare HXR emission is seen at a later time (Figure 11). We tentatively identify this weak emission as the X–ray signature of the escaping type III electrons.

These escaping electrons can be used to unambiguously trace magnetic field lines, through imaging by RHESSI of the X-rays they produce, with radio tracking of the Type III emission they produce from the Sun to 1 AU, and then detection of the electrons themselves by the Wind 3D Plasma and Energetic Particle experiment, which provides unique coverage of these ~keV to few tens of keV electrons (see Fig. 1).

Analysis of the observed velocity dispersion at onset of these electrons gives the field line length and solar release time of the detected electron beam. Furthermore, the observed spectrum of the escaping electrons can be compared with the spectrum of the electrons at the Sun inferred from the RHESSI X-ray measurements, to study the physics of the escape process. ACE and Wind ion observations can identify SEP events that are highly enriched in $^3$He. The tracking described above can identify the solar source regions, to see what conditions lead to the strong elemental and isotopic enhancements seen in $^3$He-rich events. Since these impulsive events occur frequently, these techniques can also be used for tracing the magnetic connection back to the Sun of structures such as CMEs and magnetic clouds (Larson et al 2000).

### 3.6 Other RHESSI Science

The thin walls of RHESSI's cryostat expose it to photons over 30 keV from the entire sky, and a wealth of non-solar science is already being done. RHESSI provides the largest effective area, high spectral resolution (~keV) measurements for all sky observations. In its first year of operation, RHESSI has made the first-ever measurement of polarization in a cosmic gamma-ray burst (Coburn and Boggs 2003); surprisingly, the polarization was between 50% and 100% over the energy range ~0.15-2 MeV, implying that the emission mechanism is synchrotron radiation in a region with a nearly uniform field. RHESSI is able to measure polarization because photons in this energy range Compton scatter in one detector and are stopped in another. Since every energy loss is timed to a microsecond, coincident events in two detectors can be identified. The direction of the scatter depends on the plane of the photon's electric field.

Polarization of solar flare bremsstrahlung X-rays in this energy range can also be detected in the same way, but the degree of polarization is expected to be much lower and thus are harder to detect. The hard X-ray emission from any bremsstrahlung source will be polarized if the distribution of electrons is anisotropic. RHESSI is also capable of measuring the polarization of 20-100 keV hard X-rays from solar flares. This capability arises from the inclusion of a small Beryllium (Be) scattering element that is strategically located within the cryostat that houses the array of nine GeDs. The GeDs are segmented, with both a front and rear active volume. Low energy photons (below about 100 keV) can reach a rear segment of a GeD only indirectly, by scattering. Low energy photons from the Sun have a direct path to the Be and have a high probability of Compton scattering into a rear segment of a GeD. The azimuthal distribution of these scattered photons carries with it a signature of the linear polarization of the incident flux. Sensitivity estimates, based on Monte Carlo simulations and in-flight background measurements, indicate that a 20-100 keV polarization sensitivity of less than a few percent can be achieved for X-class flares (McConnell et al., 2002).

RHESSI demonstrated its capability for detecting gamma-ray lines from impact of SEPs on Earth's atmosphere during the 21 April 2002 event. De-excitation lines from 14N and from spallation products such as 12C were detected with the polar region in view, even though the proton intensity was 10 - 100 times weaker than previously detected gamma-ray events observed by SMM and Yohkoh (Share et al., 2002). Comparison of gamma-ray line ratios provides information on the spectrum of the incident protons.

Schmahl and Hurford (2002) have developed Fourier techniques that provide a robust way of determining the spatial scales of hard X-ray flares observed using the RHESSI instrument. In a preliminary study, unpixelized forward-fitting was used to show that, in addition to the 'core' structures that the other RHESSI imaging algorithms find, there are often `halo' structures with sizes up to ~40". These 'halos' contain from 10 to 25% of the total flux in the 12-25 keV band, and may be the result of albedo emission--Compton scattering of the primary hard X-rays from the photosphere. If so, it would provide a direct indication of the height of the core x-ray emission. This can be tested by determining the energy and longitude dependence of the halo properties, and by determining the photon spectrum of the halo emission for comparison with theoretical calculations of albedo emission. These studies will also provide determinations of the dependence of core sizes on photon energy for comparison with models of downward magnetic convergence expected in beam models.

In addition, RHESSI's high sensitivity and ~1-keV (FWHM) energy resolution allow the intensity and mean energy of the iron-line complex at ~6.7 keV to be measured and imaged as a function of time. This line complex is due mostly to the 1s-2p transitions in He-like and H-like iron, Fe XXV and Fe XXVI, respectively, with associated satellite lines. Another weaker emission feature at ~8 keV made up of He-like nickel and more highly excited Fe XXV lines is also evident in the more intense flares. These measurements provide information on hot thermal flare plasmas.

## ACKNOWLEDGEMENTS

We wish to acknowledge the efforts of the entire RHESSI team in making this mission a success. This research at UCB was funded in part by NASA contract NAS5-98033.

## REFERENCES

1. Alexander, D. and Metcalf, T. R., *Astrophys. J.*, **489**, 422, 1997.
2. Aschwanden, M. J. et al., *Astrophys. J.*, **535**, 1047, 2000.
3. Aschwanden , M. J. et al., *Solar Phys.*, **210**, 193, 2002.
4. Benz, A. O. and Grigis, P. C., *Solar Phys.*, **210**, 431, 2002.
5. Brown, J. C. et al., *Solar Phys*, **210**, 373, 2002.
6. Cane, H. V. et al., *J. Geophys. Res.*, **107**, SSH14-1, CiteID 1315, 2002.
7. Coburn, W. and Boggs, S., *Nature*, in press, 2003.
8. Crosby, N. B. et al., *Solar Phys.*, **143**, 275, 1993.
9. Drake, J. F. et al., *Science*, **299**, 873, 2003.
10. Emslie, A.G., *Astrophys. J. Lett.*, in press, 2003.
11. Gallagher, P.T. et al., *Solar Phys.*, **210**, Nos. 1-2, 341, 2002.
12. Gallagher, P. T. et al., *Astrophys. J.*, **588**, 53, 2003.
13. Golpaswamy, N. et al., *Astrophys. J.*, **572**, 103, 2002.
14. Gordovsky, M. and Zharkova, V.V., National Astronomy Meeting (NAM), Dublin, Ireland, 2003.
15. Holman, G. D. et al., *Astrophys. J. Lett*, in press, 2003.
16. Hurford, G. H. and Curtis, D., *Solar Phys.*, **210**, 101, 2002.
17. Hurford, G. et al., *Solar Physics,* **210**, 61, 2002.
18. Hurford , G.J. et al., *Astrophys. J. Lett.*, in press, 2003.
19. Hurley, K., BAAS, **201**, 69.01, 2002.
20. Johns, C. M. and Lin, R. P., *Solar Phys.*, **137**, 121, 1992.
21. Kahler, S., *Astrophys. J.*, **428**, 837, 1999.
22. Kane, S. R. and Anderson, K. A., *Astrophys. J.*, **162**, 1003, 1970.
23. Klein, K.-L. and Trottet, G., *Space Sci. Rev.*, **95**, 215, 2001.
24. Kosugi et al., *Solar Physics*, **136**, 17, 1991.
25. Krucker, S. et al., *Solar Phys.*, **210**, Nos. 1-2, 445, 2002.
26. Krucker, S. et al., *Astrophys. J. Lett.*, in press, 2003.
27. Larson, D. et al., AGU, Spring Mtg, abstract #SH61A-09, 2000.
28. Lin, R. P., *Solar Phys.*, **100**, 537, 1985.
29. Lin, R. P., *Reviews of Geophysics*, **25**, 676, 1987.
30. Lin, R. P., EOS Trans, AGU, **75**, #40, 457, 1994.

31. Lin, R. P. and Hudson, H.S., *Solar Phys.*, **50**, 153, 1976.
32. Lin, R. P. et al., *Astrophys. J. Lett.*, **251**, L109, 1984
33. Lin, R. P. et al., *Geophys. Res. Lett.*, **23**, 1211, 1996
34. Lin, R. P. et al., *Astrophys. J. Lett.*, **557**, 125, 2001.
35. Lin, R. P. et al., *Astrophys. J. Lett.*, in press, 2003.
36. Makishima et al., *New Instrumentation for Space Astronomy,* K. A. van der Hucht and G. Vaiana eds., New York: Pergamon Press, 1977.
37. Mandzhavidze, N. et al., *Astrophys. J.*, **518**, 918, 1999.
38. McConnell, M. L. et al., *Solar Phys.*, **210**, Nos. 1-2, 125, 2002.
39. Murphy, R. J. et al., *Astrophys. J.*, 371, 793, 1991.
40. Oieroset, M. et al., *Physical Sci. Rev.*, **89**, id. 195001, 2002.
41. Piana, M. et al., *Astrophys. J. Lett.*, in press, 2003.
42. Prince, T.A. et al., "Gamma-Ray and Hard X-Ray Imaging of Solar Flares", *Solar Phys.*, **118**, 269, 1988.
43. Rauscher, E. et al., AGU Fall Mtg., abstract #SH52A-0482, 2002.
44. Reames, D. V., *Astrophys. J. Lett.*, **466**, 473, 1996.
45. Reames, D. V. et al., *Astrophys. J. Lett.*, **292**, 716, 1985.
46. Schmahl, E. J. and Hurford, G. J., *Solar Phys.*, **210**, Nos 1-2, 287, 2002.
47. Schwartz, R. A. et al., *Solar Phys.*, **210**, 165, 2002.
48. Share, G. H. et al., *Solar Phys.*, **210**, Nos. 1-2, 2002.
49. Share, G. H. et al., *Astrophys. J. Lett.*, in press, 2003
50. Shimizu, T., PASJ, **47**, 251, 1995.
51. Smith, D. M., *Astrophys. J. Lett.*, in press, 2003.
52. Smith, D. M. et al., *Astrophys. J. Lett.*, in press, 2003
53. Zehnder, A. et al., COSPAR Colloquia Series, *Adv. Space Res.*, in press, 2002.